Amorphous Alloy and Its Application to Joining†

Masaaki NAKA* and Ikuo OKAMOTO**

Abstract

Production methods, glass-forming conditions and fundamental properties of amorphous alloys that are produced by melt-spinning methods are reviewed, and the application of amorphous alloys to joining fields is surveyed. The merits of amorphous alloys are discussed in comparison with crystalline alloys. In particular, amorphous alloys are applied to the brazing and soldering fillers that impart the high reliability to joints. Bulky amorphous materials are tried to be prepared by laser, electron-beam melting and sputtering etc.

KEY WORDS: (Amorphous Alloys) (Non-Crystalline Alloys) (Glassy Alloys) (Amorphous Filler Metals) (Brazing) (Joining) (Melt-Spinning) (Coating)

1. Introduction

Nowdays, the usual alloys with a high periodical crystalline structure possess wide actual application. Wide efforts, on the other hand, expend towards the fields of amorphous alloys (non-crystalline alloys or glassy alloys) that possess no long periodicity from the fundamental and applicable view points. About 140 years ago, Wurtz, first, prepared the non-electroplated amorphous nickel films[1]. The electrochemical method was not developed from the actual production problems. In 1960, Duwetz et al. at CALTECH. Univ.[2] have prepared the amorphous Au-Si alloys by ejecting the molten alloys on a copper plate. The amorphous alloy showed the similar X-ray diffraction pattern as that of the liquid alloy with the same composition. This result is attributable to the recent development in the fields of amorphous alloys. This review describes the production methods, glass forming conditions, characteristics of amorphous alloys and its application to joining fields.

2. Production Methods and Glass-Forming Conditions.

Amorphous alloys are formed by suppressing its crystallization from the liquids below the glass transition temperature through the rapid quenching. The three main methods to produce amorphous alloys are shown in **Fig. 1**.

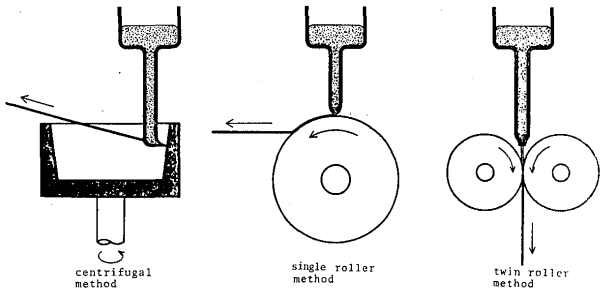

Fig. 1 Rapid quenching methods

These are the centrifugal, single roller and twin rollers[3]. The liquid alloys in the processes are ejected and quenched on the surface of the highly rotating wheel from the nozzle of quartz tube. The single roller method is often used from the easiness of production. The thickness of ribbons in the single roller method, t, is given as $t = Q^{1-n}/cV^n$, where $n = 0.8$[4]. The quenching rate of ribbon of 50 μm in thickness is estimated to be 10^6 °C/sec. The amorphous alloys in special shapes are also prepared. For instance, the amorphous wires are produced by ejecting the liquid alloy into the liquid quenching layer that is centrifugally maintained[5]. The amorphous powders are produced by means of cavitation method[6] (**Fig. 2**) or centrifugal-water method[5]. In the cavitation method the liquid is ejected between two rollers, and powdered by a cavitation with an change in pressure in liquid alloys. The powdered liquids are ejected on the surface of rotating

† Received on October 31, 1985
* Associate Professor
** Professor

Transactions of JWRI is published by Welding Research Institute of Osaka University, Ibaraki, Osaka 567, Japan

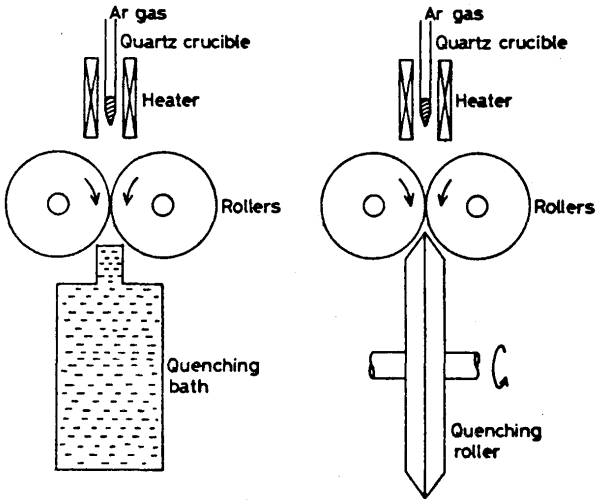

Fig. 2 Cavitation method.

wheel. The amorphous powders possess the merits of producing bulky materials by pressing, and the application to catalysis.

In order to form the liquid alloy to be amorphous the liquid is quenched below the glass transition temperature by preventing the nucleation and growth of crystal from the liquid. In the case of homogeneous nucleation and growth of crystalline phase from liquid the volume fraction of crystal is given as follows[7].

$$X = \frac{\pi}{3} I u^3 t^4 \qquad (1)$$

where I; frequency of homogeneous nucleus, u; velocity of crystal growth, t; time.

$$I = \frac{N_v D}{a^2} \exp(-\Delta G^*/kT) \qquad (2)$$

where N_v; numbers of atom per unit volume, D; average diffusion constant at the interface between liquid and crystal, a; atomic diameter, ΔG^*; free energy for formation of critical nuleus, and for the glass-forming system $\Delta G^*/kT \sim 1.07/\Delta T_r^3 \cdot T_r^2$,

$$u = \frac{fD}{a} [1 - \exp(-\Delta T_r \Delta H/RT)] \qquad (3)$$

where f; area fraction of nucleus sites, ΔH; latent heat for fusion, and $\Delta T_r = (T_m - T)/T_m$ and T_m; melting pint of metal. According to Stokes-Einstein equation $D = kT/3\pi a\eta$.

Using (1), (2) and (3) the isothermal transformation diagram (T-T-T) for the nucleation of crystal from the liquid at $x = 10^{-6}$ is calculated. The critical cooling rate for glass formation, R_c, is given as $R_c = (T_m - T_n)/t_n$, that is the cooling rate contacted with the nose of T-T-T curve. **Fig. 3** represents the T-T-T curves of metal-P binary alloys. The critical cooling rate R_c is shown in **Table 1**[8]. The

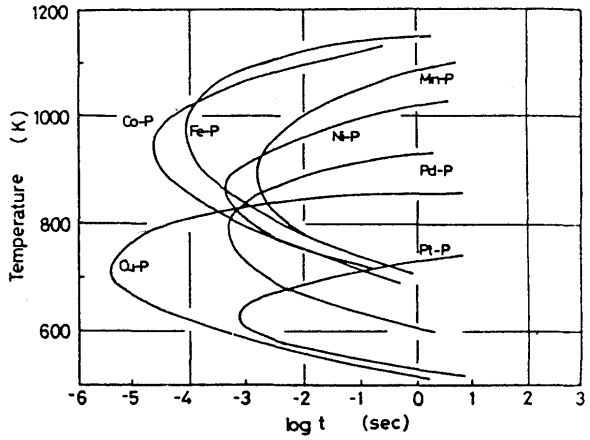

Fig. 3 T-T-T curves for crystallization of liquid alloys.

Table 1 Critical cooling rates for glass-forming ability for metal-phosphorus binary alloys, R_c.

Alloy composition	R_c (K/s)
$Mn_{86.9}P_{13.1}$	2.0×10^5
$Fe_{82.5}P_{17.5}$	4.6×10^6
$Co_{80.1}P_{19.9}$	1.4×10^7
$Ni_{81}P_{19}$	6.3×10^5
$Cu_{83.9}P_{16.1}$	7.4×10^7
$Pd_{81}P_{19}$	5.4×10^5
$Pt_{80}P_{20}$	3.3×10^5

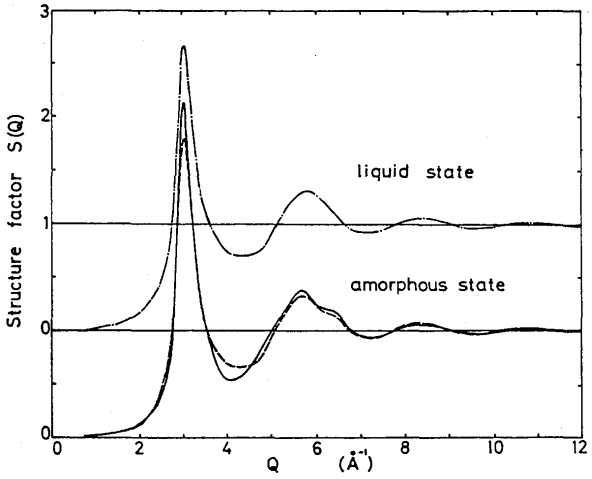

Fig. 4 Structure factors of amorphous and liquid $Ni_{80}P_{20}$ alloys.

structure of amorphous metal has become of interest in recent years. The amorphous state is regarded as the instantaneously quenched state of the liquid. The structure of amorphous state is more dense than that of liquid state because of the regularity in atomic short range order of amorphous state. **Fig. 4** shows the structure factor of amorphous and liquid $Ni_{80}P_{20}$ alloys.[9]

3. Characteristic Properties of Amorphous Alloys

One of outstanding characteristics is a high strength of amorphous alloys. For instance, the tensile strength and hardness of $Fe_{80}B_{20}$ are 370 kg/mm^2 and 1100 kg/mm^2, respectively. The tensile strength of $Fe_{80}B_{20}$ is comparable to 300 kg/mm^2 of commercial piano wires. Amorphous alloys are high strength materials. The relative strength ratio (E/σ_y) of amorphous $Fe_{80}B_{20}$ is comparable to that of other typical high strength materials in **Table 2**[1], where E and σ_y are the elastic constant and yield stress, respectively. The value of $Fe_{80}B_{20}$, 45, is comparable to other high strength materials.

The hardness is a measure of strength, and the ratio of hardness (H_v) to strength (σ) for amorphous alloys is about 2.5 ~ 3, and corresponds to the non-strain hardening value, 2.9, of ideal elastic materials. Fig. 5 shows the hardness of a variety of amorphous iron alloys[10].

The amorphous alloys are electro-chemically homogeneous and, free from crystalline boundaries and segregates which are nucleus sites of corrosion. The alloys are high concentrated solid solutions that could not be attained in crystalline alloys. From the above facts amorphous alloys show extraordinary chemical characteristics.

Table 2 Relative strength ratio (E/σ_y) of high strength materials.

Materials	E/σ_y
$Fe_{80}B_{20}$ amorphos alloys	45
Fe Whisker	15.5
SiC	33.3
AlN	50
B filament coated on W	55

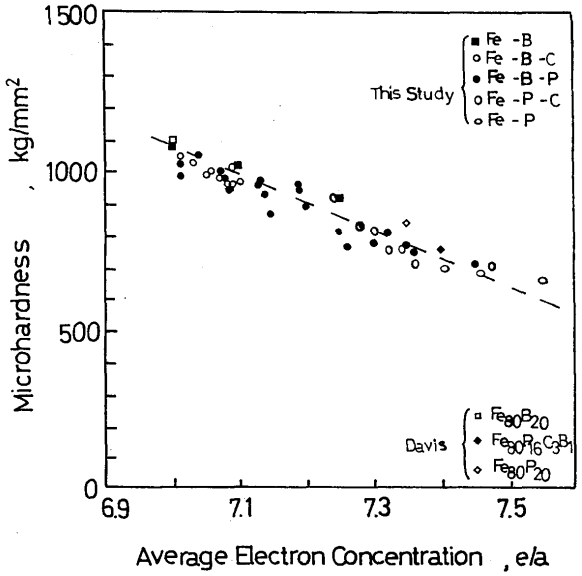

Fig. 5 Microhardness of amorphous $Fe_{80}(B,P)_{20-x}M_x$ alloys plotted against e/a.

Fig. 6 shows corrosion rates of amorphous Fe-Cr-P-C alloys in 1N NaCl.[11] Included in the figure are shown the values of crystalline Fe-Cr binary alloys. Although usual crystalline stainless steels are easily corroded due to pitting corrosion in solutions containing chrolide, amorphous Fe-Cr-P-C alloys exhibit a extremely high corrosion resistance. A large amount of phosphorus gives rise to the high chemical activity of matrix alloy which are necessary to form the protective hydrated chromium oxyhydroxide. Further, amorphous alloys with small amounts of defects are electrochemically homogeneous. These give rise to the high corrosion resistance of the alloys. In particular, $Fe_{80}Cr_{10}P_{13}C_7$ alloy is self-passivated in 1N HCl. The outstanding effect of phosphorus is also revealed in **Fig. 7**[12].

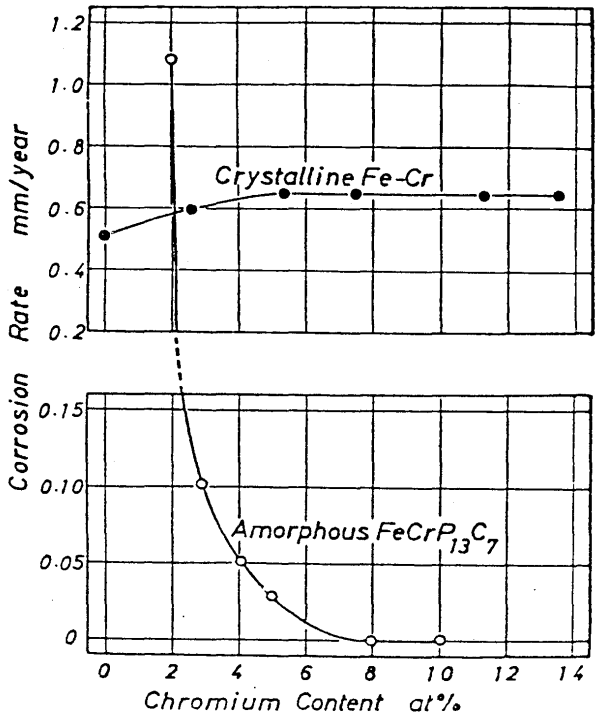

Fig. 6 Corrosion rates of amorphous $Fe_{80-x}Cr_xP_{13}C_7$ alloys in 1N HCl.

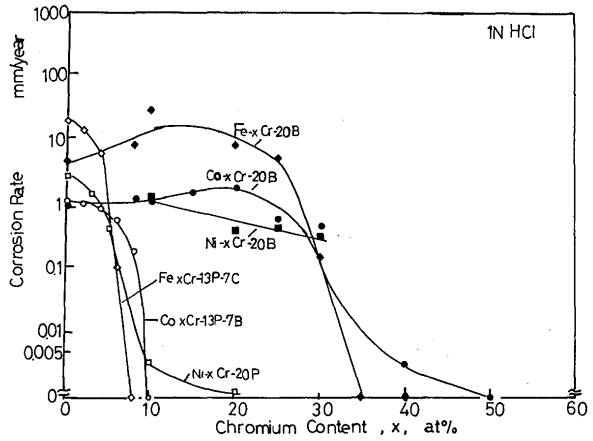

Fig. 7 Corrosion rates of a variety of amorphous alloys in 1N HCl.

4. Application to Filler Metals

4.1 Titanium base amorphous filler metals

The method of joining ceramics reported are mainly concentrated on oxide ceramics as follows; (1) solid state diffusion bonding (including gold metal method), (2) active alloy method, (3) high refractory alloy method (Mo-Mn), and (4) metal-metal oxide eutectic method. These methods are often complex joining methods, and possess severe joining conditions. Compared with these methods, the application of amorphous filler alloys exhibits a simplicity of joining process due to its flexibility and homogeneity of compositions. **Table 3** shows the alloy composition, liquid temperature, and thickness of titanium base filler metals.[13] The amorphous fillers are about 45 μm thick and 1 ~ 50 mm wide. The appearance of the filler and inner parts of quenching apparatus are shown in **Figs. 8** and **9**, respectively.

A good wetability is necessary for joing of ceramics to metals. **Fig. 10** shows a change in equilibrium contact angle of Cu-Ti alloys on Al_2O_3 or Si_3N_4 with titanium content at 1100°C. The titanium content in the filler is desired to be higher than 30 atomic percent. **Fig. 11** shows the brazing temperature dependence of Al_2O_3/Cu joint at constant brazing time of 30 min. **Fig. 12** represents the brazing time dependence of Al_2O_3 joint at constant brazing temperature[14]. The joining strength of the joint increases with brazing temperature, and exhibits a maximum against brazing time. Whereas a reaction at the interface of joint proceeds, the alumina itself near the interface is damaged with the proceeding of the reaction. This gives rise to the decrease in joining strength. The intermediate titanium oxide at the interface of Al_2O_3/CuTi/Cu joint is

Table 3 Characteristic properties of amorphous titanium base filler metals.

	Nominal composition (at%)			Liquidus temperature (°C)	Thickness (μm)
	Ti	Cu	Ni		
$Cu_{50}Ti_{50}$	50	50	-	975	50
$Cu_{43}Ti_{57}$	57	43	-	955	45
$Cu_{66}Ti_{34}$	34	66	-	875	45
$Ni_{24.5}Ti_{75.5}$	75.5	-	24.5	955	45

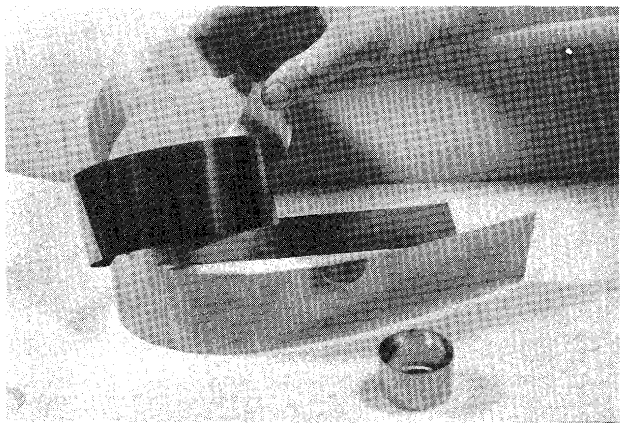

Fig. 8 $Cu_{50}Ti_{50}$ amorphous filler alloy.

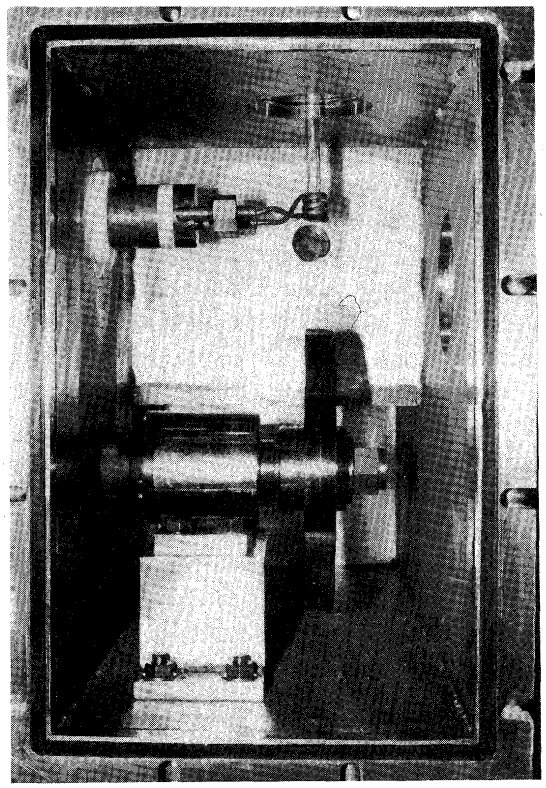

Fig. 9 Inner parts of quenching apparatus.

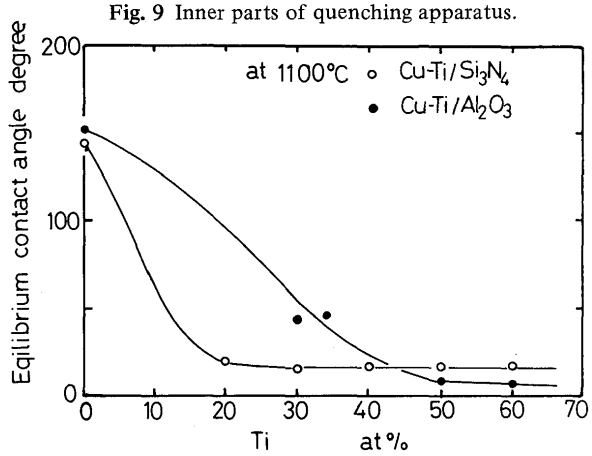

Fig. 10 Equilibrium contact angles of Cu-Ti liquid alloys on Al_2O_3 or Si_3N_4 at 1100°C.

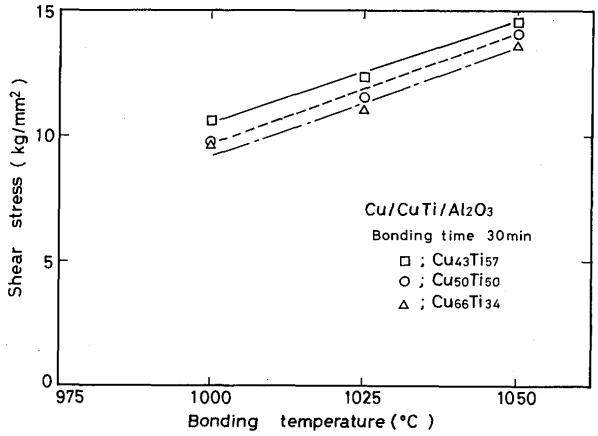

Fig. 11 Brazing temperature dependence of joining strength of Al_2O_3/Cu joint at constant brazing time of 30 min.

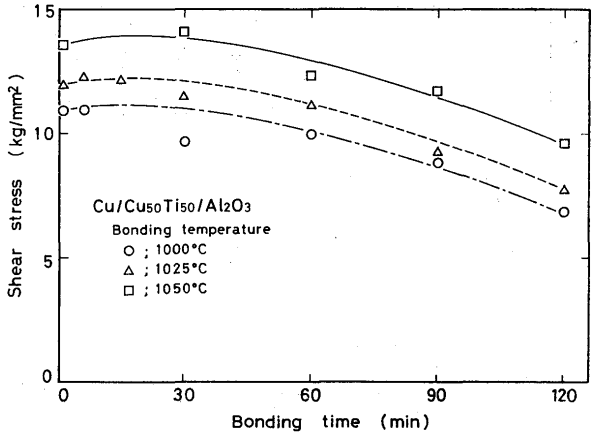

Fig. 12 Brazing time dependence of joining strength of Al_2O_3/Cu joint at constant brazing temperatures.

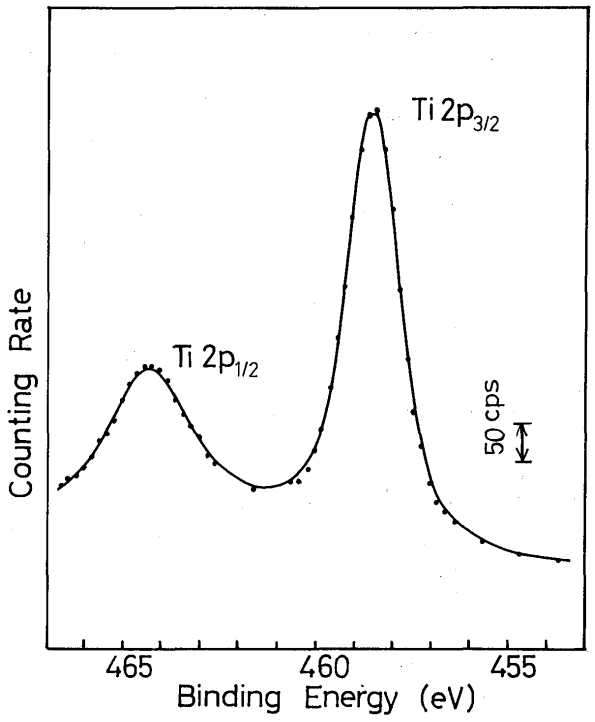

Fig. 13 Ti2p spectra of revealed interface of Al_2O_3.

revealed using XPS analyser in **Fig. 13**, and the structure of joint is shown in **Fig. 14**. A small amount of titanium dissolves in Al_2O_3 and TiO_x is formed in the interface. The SEM microstructure of Al_2O_3/Cu joint is shown in **Fig. 15**. The isothermal solidification process takes place during joining. Copper, first, dissolves into Cu-Ti liquid filler, and then copper solid solution containing titanium precipitates from the filler. The liquid filler gradually dissolves into copper by the process.

The thermal expansion coefficient of material takes an important role in joining ceramics to metals. For instance, Kovar alloy (54%Fe, 24%Ni, 17%Co) that possesses the similar expansion coefficient of $\alpha = 6.0 \times 10^{-6}/°C$ to $\alpha = 8.1 \times 10^{-6}/°C$ of Al_2O_3. The brazing temperature dependence of joining strength for Al_2O_3/CuTi/Kovar

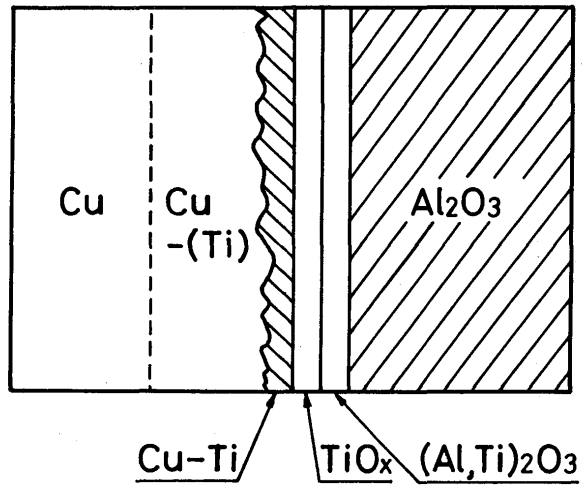

Fig. 14 Schematic structure of Al_2O_3/CuTi/Cu joint.

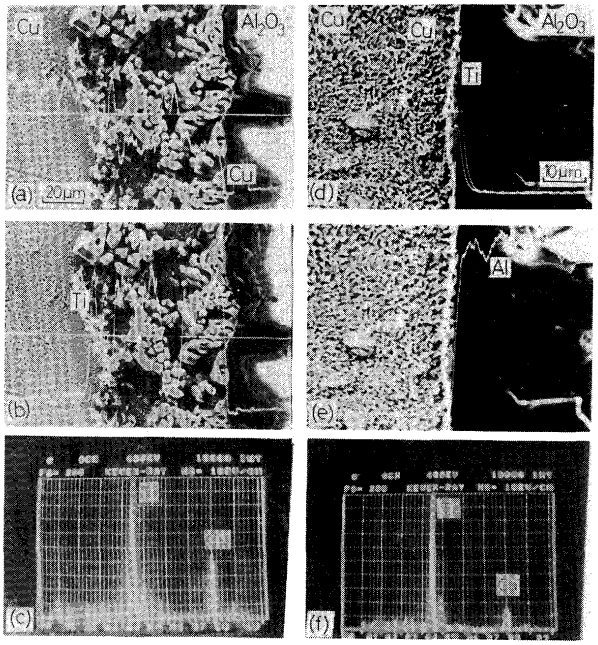

Fig. 15 Microstructures of Al_2O_3/CuTi/Cu at 1000°C (a, b, c) and 1050°C (d,e,f).

joint is shown in **Fig. 16**, and the structure of interface is given in **Fig. 17**[14]. The joining strength of Al_2O_3/Kovar joint is higher than that of Al_2O_3/CuTi/Cu joint.

The wide interests recently focus on the cobalently bonded nonoxide ceramics because the non-oxide ceramics possess high strength, compared with that of oxide ceramics (The bending strength; $Si_3N_4 = 50\ kg/mm^2$, $Al_2O_3 = 30\ kg/mm^2$). The joining strength of Si_3N_4/Si_3N_4 joint is plotted against the brazing temperature using Cu-Ti filler metal[15] in **Fig. 18**. The joint made with Cu rich $Cu_{66}Ti_{54}$ filler provides high joining strength compared with other fillers except for the case of brazing at 1000°C. At the interface of the joint TiN, Ti_5Si_3, ϵ-$Cu_{15}Si_4$, η-(Cu, Si) are formed. The growth of TiN which is formed at the interface of Si_3N_4 are dominated by the diffusion of N in TiN. During brazing the filler divides

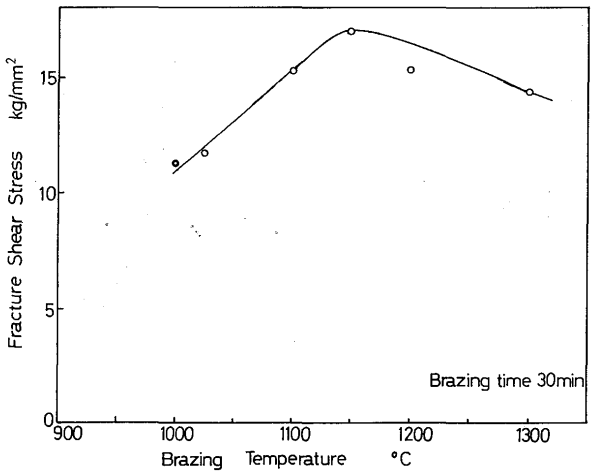

Fig. 16 Brazing temperature dependence of joining strength of Al_2O_3/CuTi/Kovar joint at constant brazing time of 30 min.

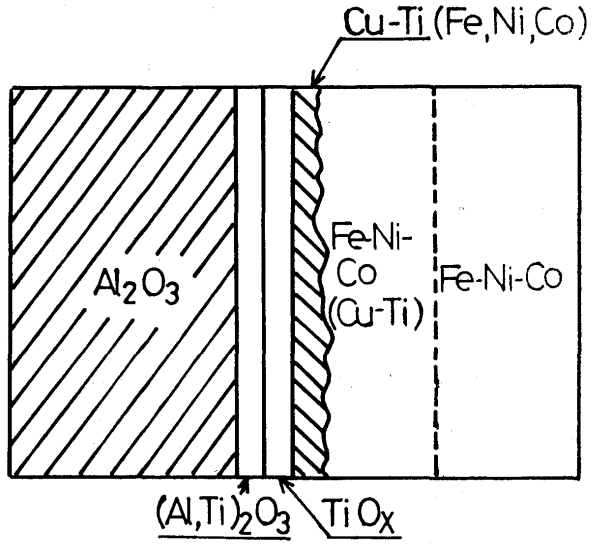

Fig. 17 Schematic microstructure of Al_2O_3/CuTi/Kovar joint.

into the titanium-rich layer on the ceramics side and the copper-rich layer on the inner filler side. The silicon content in the copper rich side increases with increasing the brazing temperature. The testing temperature dependence of joining strength of various kinds of joints is represented in **Fig. 19**. The joint of Si_3N_4/Si_3N_4 maintains the strength up to 700°C because of its the dispersion hardening of silicides in the filler.

The characteristics of amorphous filler metals are as follows.

(1) The amorphous filler can be punched out into the desired size or can be bent to counter parts because of its high flexibility that comes from amorphous structure. The accuracy of joining dimension and the joining strength are improved by using the amorphous filler because the brazing is made by inserting the filler into the joining interface. On the other hand, the usual joining is made with the titanium base power filler containing embritteled intermetallic compounds

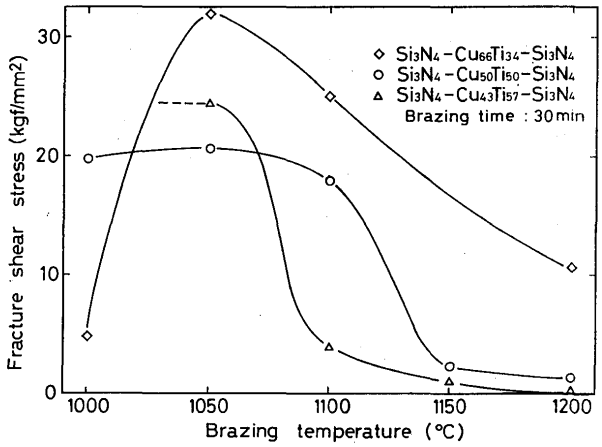

Fig. 18 Brazing temperature of joint strength of Si_3N_4/CuTi/Si_3N_4 joint at constant brazing time of 30 min.

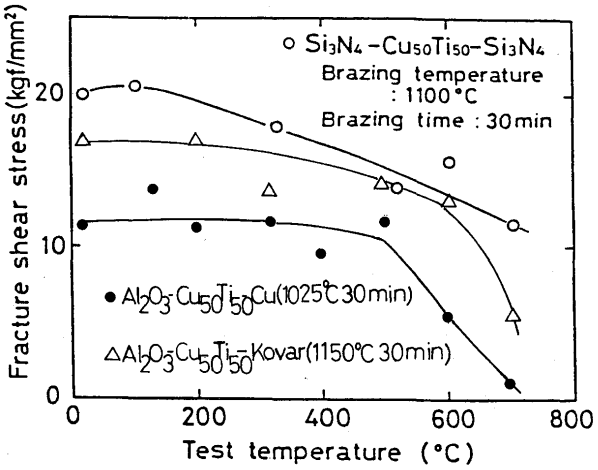

Fig. 19 Testing temperature dependence of joining strength of a variety of joint.

using the binder. This binder is attributed to the defects and voids in the joints, and results in decreasing the joining strength.

(2) Amorphous alloys are a kind of solid solution, and provide the homogeneity of joining parts. On the other hand, the multiple phases in the usual filler provides the inhomogeneity of the joining layer. **Figs. 20** and **21** show the reliability of Al_2O_3/Cu joint using amorphous and crystalline fillers. The standard deviations of joining strength are 3.2 kg/mm² and 4.6 kg/mm² for the amorphous and crystalline fillers, respectively, where the joining was made at 1025°C for 30 min. The deviation of strength using the powder filler is large.

4.2 Amorphous nickel base filler metals

Table 4 show the chemical compositions, liquidus and solidus temperature and brazing temperature (produced by Allied Co.)[16,17]. These filler metals correspond to the usual nickel fillers (BN-1, -2, -3, -6). The diffusion of boron is fast in joining with amorphous filler, and this results in the homogeneity of boron in the joint. **Figs. 22** and **23** show the distribution of elements in SUS316

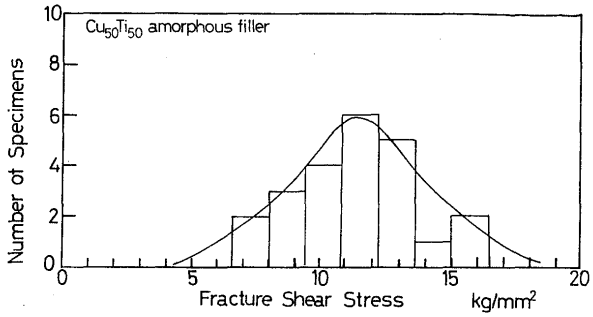

Fig. 20 Scattering of strength values of Al_2O_3/Cu joints made with amorphous filler.

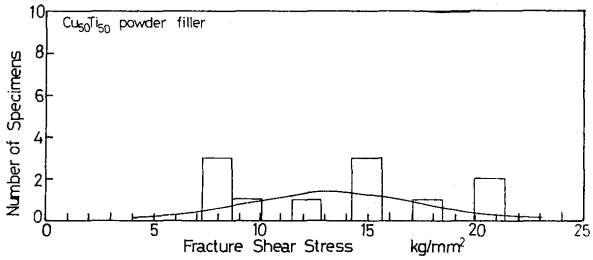

Fig. 21 Scattering of strength values of Al_2O_3/Cu joints made with crystalline powder filler.

Table 4 Characteristic properties of amorphous nickel base filler metals.

	Nominal composition(wt%)	JIS	Solidus temp (°C)	Liquidus temp (°C)	Flow temp (°C)
MBF-10	$Ni_{Bal.}$, Cr_{14}, $Fe_{4.5}$, $Si_{4.5}$, $B_{3.2}$, $C_{0.06}$	JIS BNi-1	970	1040	1060~1080
MBF-15	$Ni_{Bal.}$, Cr_{13}, $Fe_{4.2}$, $Si_{4.5}$, $B_{2.8}$, $C_{0.03}$		960	1125	1080~1095
MBF-20	$Ni_{Bal.}$, Cr_{7}, $Si_{4.5}$, Fe_{3}, $B_{3.2}$	JIS BNi-2	970	1000	1010~1030
MBF-30	$Ni_{Bal.}$, $Si_{4.5}$, $B_{3.2}$	JIS BNi-3	980	1040	1040~1070
MBF-60	$Ni_{Bal.}$, P_{11}	JIS BNi-6	880	880	925 (1700)
MBF-75	$Ni_{Bal.}$, Cr_{10}, $Fe_{5.5}$, $Mo_{0.7}$, $C_{0.23}$, $B_{3.5}$		1057	1165	1175~1205
MBF-80	$Ni_{Bal.}$, $Cr_{15.2}$, $B_{4.0}$		1020	1065	1065~1095

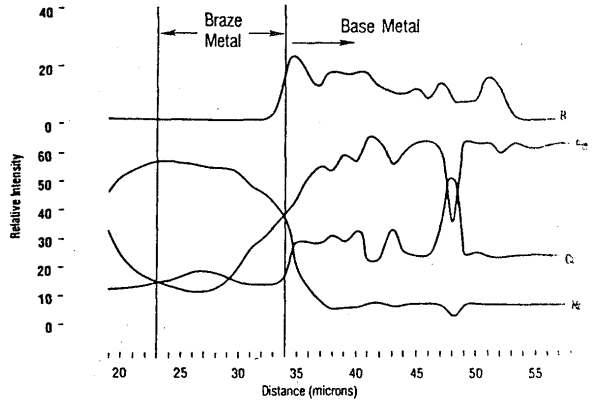

Fig. 22 Line analyses of elements of SUS316 joint made with amorphous nickel filler.

joint using MBF-20 amorphous and BNi-2 powder filler. The homogeneity of the joint with BNi-2 is low and boron forms $(Cr, M)_2B$ in the filler. In the joint with amorphous filler B and Cr dissolve homogeneously into the matrix[18]. Amorphous filler metals are applied to brazing compressor stators of jet engine and air sheals in the honeycombs **(Fig. 24)** for the high temperature heat exchange and

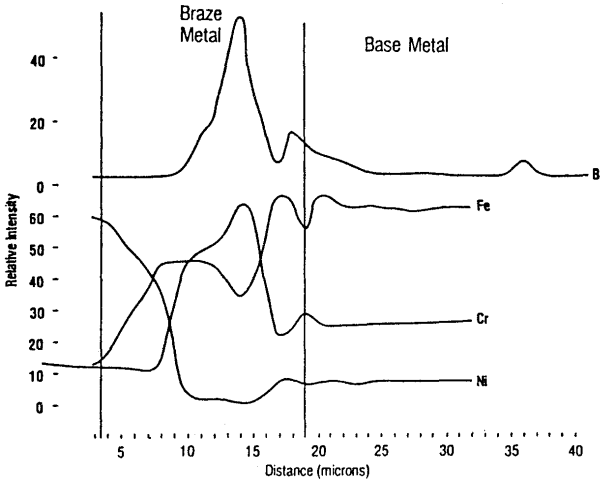

Fig. 23 Line analyses of elements of SUS316 joint made with BNi-2 powder.

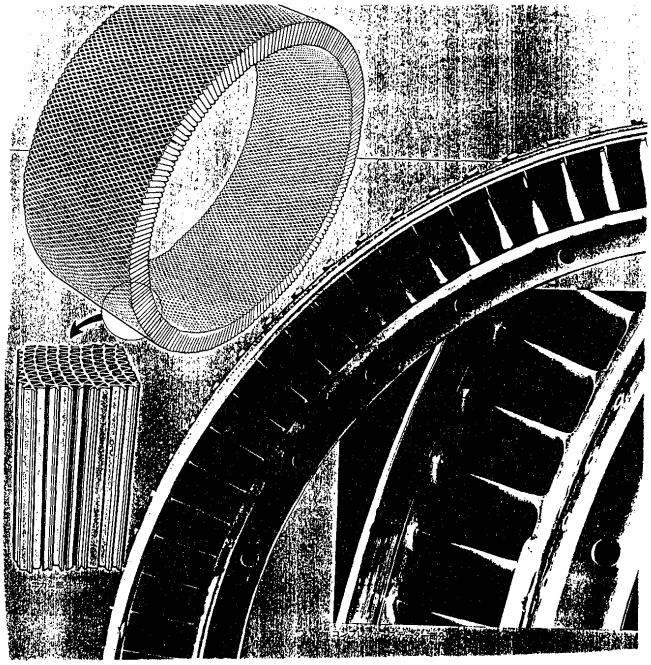

Fig. 24 Parts of stator of jet engine and honeycomb structure.

relaxation structures[16].

4.3 Amorphous copper base filler metals

Table 5 gives the chemical compositions and fundamental parameters of the filler metals produced by Allied Co.[17]. The content of phosphorus is the same as the usual filler, but the high content of Ni and Sn up to about 10 wt% makes possible to braze at temperature of 100°C lower than the usual brazing temperature. Phosphorus plays the self fluxing action. Although tin promotes the spread of filler, large amounts of tin dissolve the matrix of copper. BCu-2 (Cu-6.8 ~ 7.5%P) was quenched to be crystalline ribbons using a melt-spinning method. The embrittlement of the ribbons is improved by a heat treatment at temperatures above 400°C. After the heat-treatment the ribbon can be bent into the counters and punched out. **Fig. 25** shows the appearance of the ribbon

Table 5 Characteristic properties of amorphous copper base filler metals.

	Nominal composition(wt%)				Liquidus temp (°C)	Brazing Temp. (°C)
	Ni	Sn	P	Cu		
MBF 2001	9.6	9.7	7.0	Bal	595	635
MBF 2002	9.9	4.0	7.8	〃	610	645
MBF 2005	5.7	9.7	7.0	〃	591	637

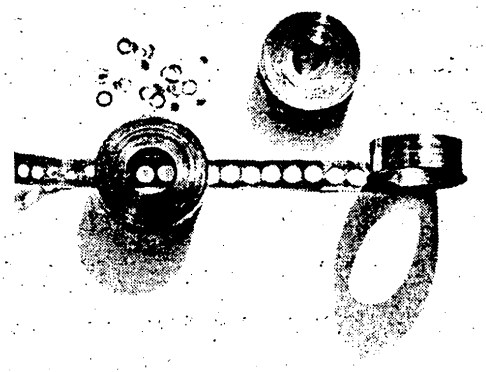

Fig. 25 BCu-P filler ribbons.

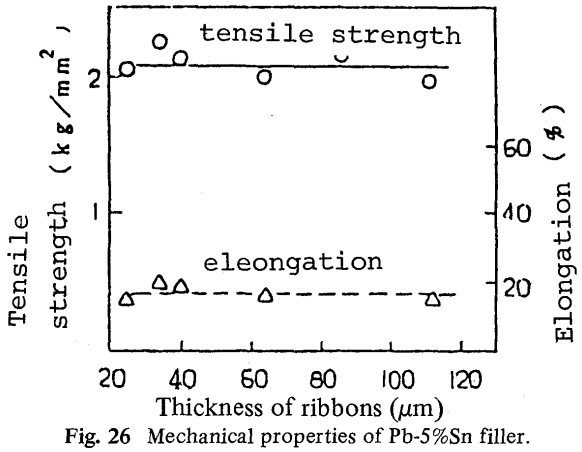

Fig. 26 Mechanical properties of Pb-5%Sn filler.

of copper filler[19].

A number of Al-Si-Mg alloys was cast into filler metal foils by a melt spinning method. The cast fillers can tolerate large amounts of alloying elements (e.g. Mg) and melting point depressor (e.g. Si) without fabrication difficulties[21]

4.4 Rapidly quenched solder

It was difficult to prepare the thin ribbon of solder below 50 μm in thickness because of its softness by usual roller method. Pb-5%Sn and Pb-6.5%Sn solder in thickness of 100 μm or less were produced by a melt-spinning method.[20] The mechanical properties of the Pb-5%Sn are shown in **Fig. 26**. The melt-spinning method also permits the fabrication of other solders such as Sn, In and Au base alloys with grain size less than 1.0 μm also shown in **Fig. 27**.[21]

5. Application to Other Fields

As the size of ribbons prepared by a melt-spinning method is limited, the formation of amorphous alloys, in particular, the high-corrosion resistant amorphous alloys that one of the present authors has found, was tried.

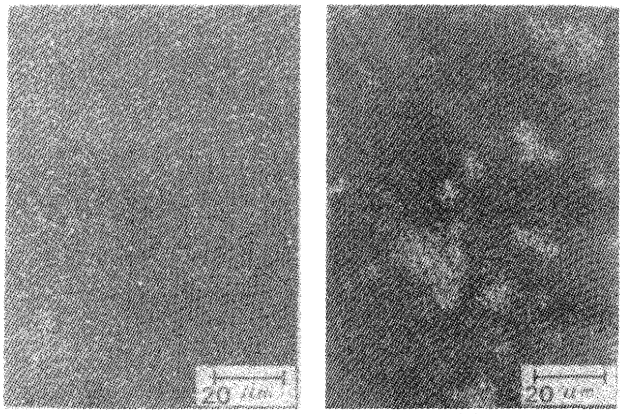

Fig. 27 SEM X-ray Ag map of 65Sn-25Ag-10Sb solder, a) melt-spinning foil, b) rolled foil.

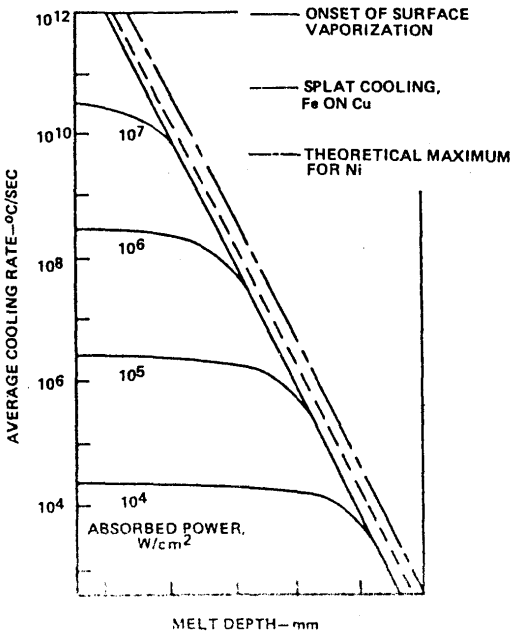

Fig. 28 Cooling rates plotted against melting depth using laser heating.

5.1 Formation of amorphous layers produced by laser surface treatment.

Small parts of the surface are melt-quenched by laser heating. **Fig. 28** shows a change in cooling rate with the melting-depth.[22] At the cooling rate of 10^6 °C/sec or more the amorphous phase will be formed. **Figs. 29** and **30** show the structure of amorphous phases.[23]

5.2 Formation of amorphous layers produced by electron-beam surface treatment

At the power of 50 ~ 200 W and the velocity of 4.36 cm/sec, the change in temperature are plotted against cooling time as a function of melting depth as shown in **Fig. 31**.[24] The quenched structures of $Fe_{80}P_{13}C_7$ alloy

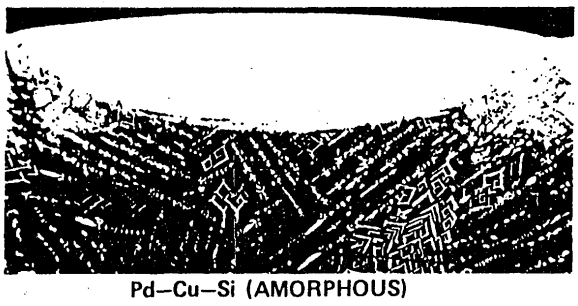

Fig. 29 Microstructure of Pd-Cu-Si alloy by laser-melting.

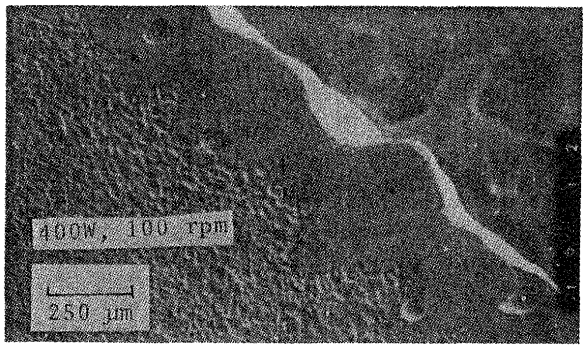

Fig. 30 Microstructure of Ni-P alloy by laser-melting.

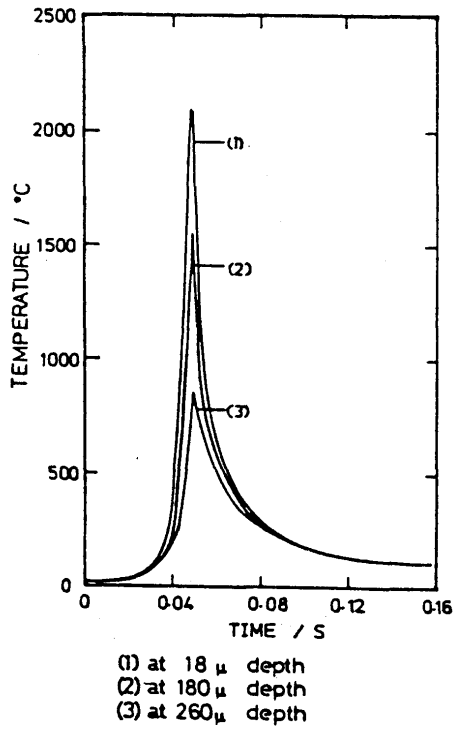

Fig. 31 Cooling rates plotted against melting depth in electron beam melting.

including the amorphous phase are shown in Fig. 32.[25]

5.3 Formation of amorphous layer is produced by spraying

Amorphous pahses are produced by spraying materials on the water-cooled copper plate. The spraying method and the foil of $Fe_{40}Ni_{40}P_{14}B_6$ amorphous alloy are shown in Figs. 33 and 34, [25,26] respectively. The sprayed alloys are Cu-Zr, Fe-Cr-Ni-P-B alloys.

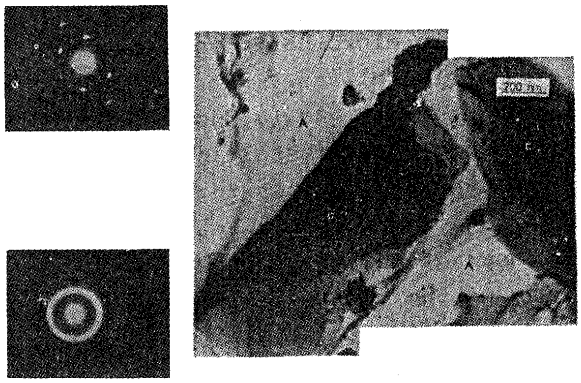

Fig. 32 Microstructure of $Fe_{80}P_{13}C_7$ alloy melted by electron beam heating.

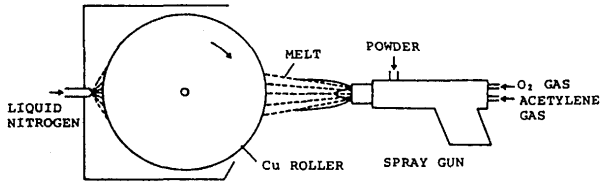

Fig. 33 Rapid quenching method by spraying.

5.4 Formation of amorphous alloys produced by sputtering

Amorphous phases are produced by sputtering materials on the water-cooled substrate. The argon ions collide with the materials. A large amount of metalloids is introduced into the amorphous matrix. Figs. 35, 36 and 37 show the sputtering apparatus, structure of Ti-B amorphous phases, the anodic polarization curves of $Fe_{60}Cr_{20}P_{13}C_7$ and $Cr_{75}B_{25}$ amorphous alloys in 1N HCl, respectively. High corrosion resistant amorphous films are produced by sputtering[27,28,29]. The hardness of amorphous Cr-C, H_V = 1288, is extremely high.

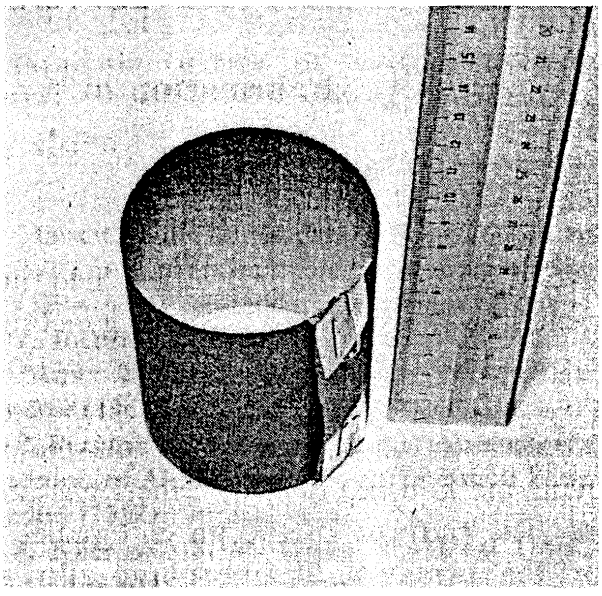

Fig. 34 $Fe_{40}Ni_{40}P_{14}B_6$ sprayed alloy.

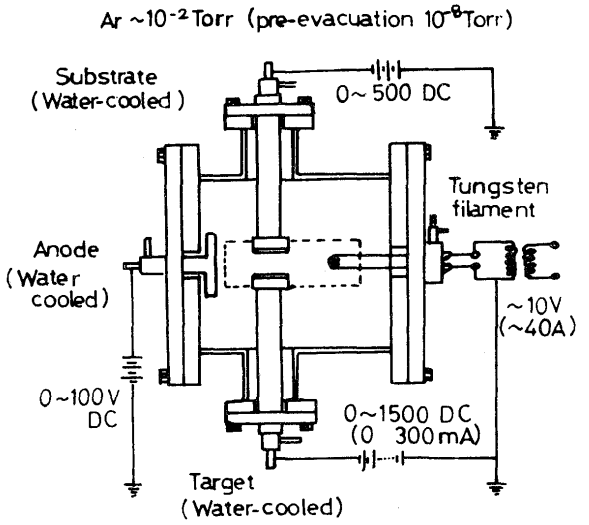

Fig. 35 Sputtering method.

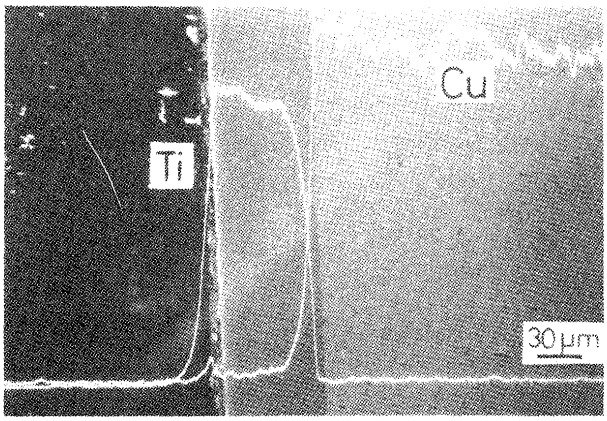

Fig. 36 Coating of amorpous $Ti_{75}B_{25}$ alloy.

5.5 Joining of amorphous alloys

Metastable phases will crystallize during static compressing the powders. On the other hand, dynamic compression makes the metastable phases to be bulky materials without crystallization. The friction among particles partly causes to melt the surface of particles, and join them. Amorphous phases are joined by ultrasonic loading in a short time. **Figs. 38, 39** and **40** shows the change in fracture loading of $Fe_{40}Ni_{40}P_{14}B_6$ with electric power input, structure of joining surface and diffraction patterns of joint, respectively.[30] The fracture load gives the maximum at 30 kHz, 0.5 sec under 20 MN/m^2. The structure of joints are amorphous as shown in **Fig. 40**.

Amorphous alloys are joined by resistant spot-welding method using short current pulses. The cange in structure of weld structure with welding condition is shown in **Fig. 41**.[31] The structure varies from fully revitrified to fully crystallized welds.

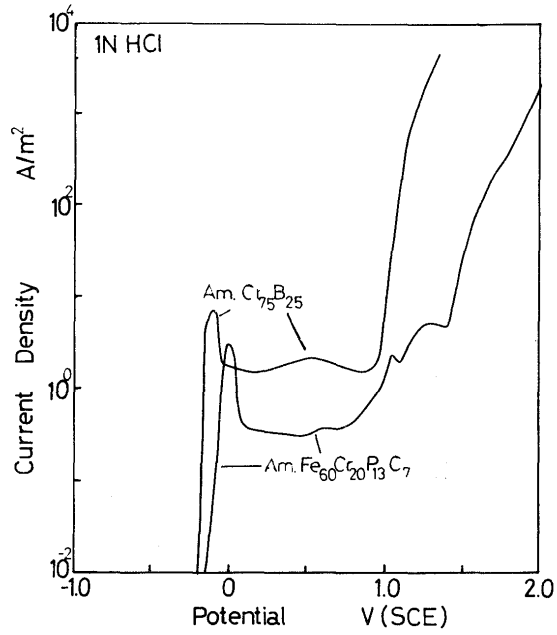

Fig. 37 Anodic polarization curves of $Fe_{60}Cr_{20}P_{13}C_7$ and $Cr_{75}B_{25}$ amorphous alloys.

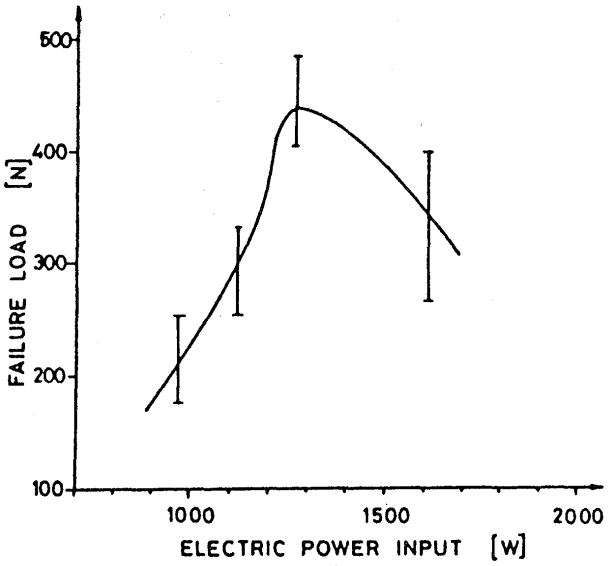

Fig. 38 Joining strength of amorphous $Fe_{40}Ni_{40}P_{14}B_6$ alloy/Cu joint.

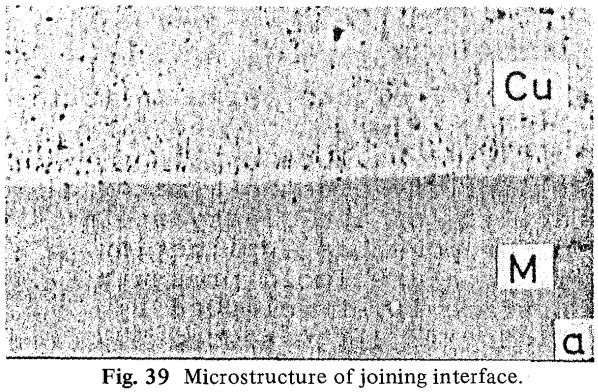

Fig. 39 Microstructure of joining interface.

6. Summary

Considerable attensions are focussed on the future materials of amorphous alloys without periodicity in the structure because of its superior properties such as mechanical, chemical properties. In Joining fields amorphous

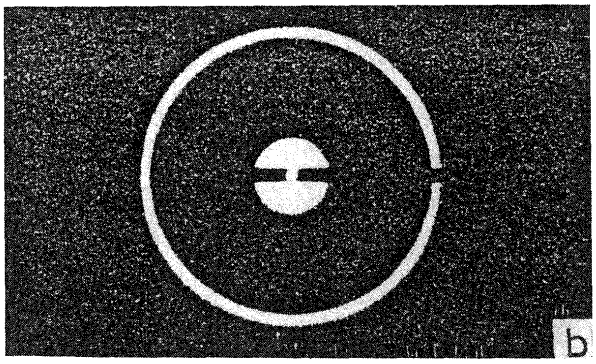

Fig. 40 Electron diffraction pattern of amorphous $Fe_{40}Ni_{40}P_{14}B_6$ alloy/Cu joint.

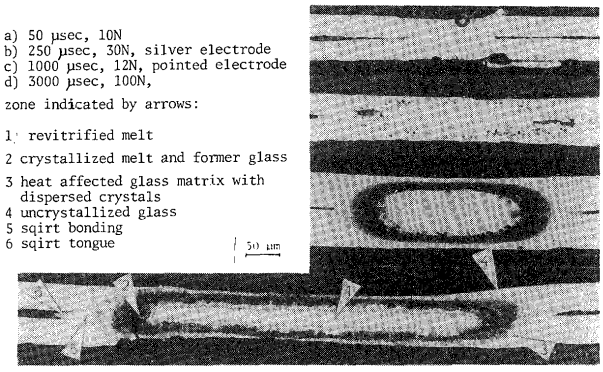

Fig. 41 Spot welded joint in amorphous $Ni_{78}Si_8B_{14}$ alloy.

filler metals possess the superior flexibility, homogeneity of composition, and provide the high reliability of joint. In order to produce the bulky amorphous alloys laser surface treatment, sputtering, explosive method were conducted. These results give rise to further applications in various field.

Finally the authors wish to thank Prof. Y. Arata, Welding Research Institute of Osaka Univeriity for encouraging to summarize this review.

References

1) Metallic Glasses, ASM (1976).

2) P. Duwetz et al., Nature, **187** (1960), 809.

3) T. Masumoto and K. Fukamichi, Amorphous Alloys, Agune (1981).

4) S. Kavesh, Metallic Glasses, ASM (1976), 36.

5) I. Onaka and T. Fukusako, J. Japan Inst. Metals, **42** (1978), 415.

6) H. Ishii, M. Naka and T. Masumoto, Sci. Rep. Tohoku Univ., A29 (1981), 343.

7) D.R. Uhlmann, J. Non-Cryst. Solids, 7 (1972), 337.

8) M. Naka, A. Inoue and T. Masumoto, Sci. Rep. Tohoku Univ., A29 (1981), 231.

9) Y. Waseda, H. Okazaki, M. Naka and T. Masumoto, Sci. Rep. Tohoku Univ., A26 (1981), 12.

10) M. Naka, T. Masumoto and H.S. Chen, J. de Physique, **41** (1980), C8-839.

11) M. Naka, K. Hashimoto and T. Masumoto, J. Japan Inst. Metals, **38** (1974). 835.

12) M. Naka, K. Hashimoto and T. Masumoto, J. Non-Cryst, Solids, **34** (1979), 257.

13) M. Naka, K. Asami, I. Okamoto and Y. Arata, Trans. JWRI., **12** (1983), No. 2, 145.

14) M. Naka, K. Sampath, I. Okamoto and Y. Arata, Proc. Int. Conf. Joining of Metals, Denmark, 1984, 168.

15) M. Naka, T. Tanaka, I. Okamoto and Y. Arata, Trans. JWRI., **12** (1983), No. 2, 177.

16) Nippon Hishoshitsu Co. Tech. Rep.

17) S. Ariga, J. Japan Welding Soc., **53** (1984), 7.

18) N. Decristofaro and C. Henschel, Welding J., (1978), 33.

19) H. Kikuchi, M. Moriguchi and K. Shiroyama, Proc. Spring Meeting. Japan Inst. Metals, (1983), 304.

20) H. Kikuchi, K. Shiroyama, Proc. Autumn Meeting. Japan Inst. Metals, (1983), 545.

21) N. Cristofaro and A. Datta, Proc. 5th Int. Conf. Rapidly Rapidly Quenched Metals, ed. by S. Steeb and H. Warlimont, 1985, 1715.

22) E.M. Breinan and B.H. Kear, Rapid Solidification Processing, Claritor's Pub., (1978), 87.

23) K. Asami, S. Sato and K. Hashimoto, Proc. 4th Int. Conf. Rapidly Quenched Metals, Japan Inst. Metals, (1982), 177.

24) A. Mawella and K. Honeycombe, ref. (23), p 185.

25) H. Shingu and R. Ozaki, Trans. JIM., **20** (1979), 33.

26) H. Mimura et al., Trans. JIM., **22** (1981), 597.

27) M. Naka, H. Fujimori, I. Okamoto and Y. Arata, Proc. 7th Int. Conf. Vacuum Metallurgy, (1982), Iron Steel Inst. Japan, p 650.

28) M. Naka, H. Fujimori, H. Hanada, I. Okamoto and Y. Arata, Trans. JWRI., **11** (1982), No. 2, 23.

29) M. Naka, S. Hanada and I. Okamoto, Proc. 5th Int. Conf. Rapidly Quenched Metals, ed. by S. Steeb and H. Warlimont, Elsevier Sci. Pub., 1985, p. 361.

30) H. Kreye, M. Hammerschmidt and G. Reiners, Scripta Met., **12** (1978), 1059.

31) S. Hock, ref. (21), p 1771.